Tellus (2008), 60B, 213–225
Printed in Singapore. All rights reserved

TELLUS

Atmospheric O_2/N_2 measurements at two Japanese sites: estimation of global oceanic and land biotic carbon sinks and analysis of the variations in atmospheric potential oxygen (APO)

By YASUNORI TOHJIMA*, HITOSHI MUKAI, YUKIHIRO NOJIRI, HIROAKI YAMAGISHI and TOSHINOBU MACHIDA, *National Institute for Environmental Studies, Tsukuba 305-8506, Japan*

(Manuscript received 5 March 2007; in final form 19 November 2007)

ABSTRACT

We present measurements of atmospheric O_2/N_2 and CO_2 mixing ratios taken at Hateruma Island (HAT) and Cape Ochi-Ishi (COI) in Japan. Global carbon sinks are estimated from the tracer atmospheric potential oxygen (APO) calculated as the weighted sums of the observed O_2/N_2 and CO_2, and the global CO_2 data from the NOAA/ESRL GMD flask sampling network. The oceanic and land biotic sinks are 2.4 ± 0.7 and 0.5 ± 0.9 Pg C yr^{-1}, respectively, for the 7-yr period (July 1998–July 2005) and 2.1 ± 0.7 and 1.0 ± 0.9 Pg C yr^{-1}, respectively, for the 6-yr period (July 1999–July 2005). The former 7-yr estimates are based on the data from HAT only, while the latter 6-yr estimates are obtained using data from both HAT and COI. These estimations include an ocean outgassing correction of 0.48 Pg C yr^{-1}. The instantaneous rates of change in the APO trends show large interannual variability with peak-to-peak amplitudes of about 30 per meg yr^{-1}. The winter anomalies in the APO trend are the major contributor to the interannual variability, and the oceanic O_2 influx associated with winter ventilation may be a significant cause of the variability in APO.

1. Introduction

Observation of the long-term change in atmospheric O_2 concentration, combined with CO_2 observation, furnishes us with additional information about the global carbon cycle. This is based on the fact that O_2 and CO_2 fluxes are tightly coupled during land biotic processes such as photosynthesis and respiration, but are not coupled during the sea–air gas exchange processes. In early atmospheric O_2 studies, the terrestrial sequestration rate of fossil fuel CO_2 was calculated simply from the difference between the observed atmospheric O_2 decrease and the expected O_2 consumption due to burning of fossil fuels on the assumption that the net oceanic O_2 flux was zero because of the relatively low solubility of O_2 in seawater (Keeling and Shertz, 1992; Bender et al., 1996; Keeling et al., 1996; Battle et al., 2000). However, to quantify the global oceanic and land biotic carbon sinks more accurately, we need to evaluate the net oceanic O_2 flux because the upper-ocean warming caused by the anthropogenic radiative forcing is expected to alter significantly the balance of O_2 inventories between the ocean and the atmosphere. More recently it has been possible to make corrections for oceanic O_2 outgassing due to ocean warming and several studies have been devoted to the evaluation of the net oceanic O_2 fluxes (Bopp et al., 2002; Keeling and Garcia, 2002; Plattner et al., 2002), but there remains large uncertainty in the estimation. In spite of these difficulties, atmospheric O_2 measurements serve as an important tool in the study of the global carbon cycle. Presently, several groups have ongoing atmospheric O_2/N_2 measurement programs (e.g. Langenfelds et al., 1999; Tohjima et al., 2003; Bender et al., 2005; Sturm et al., 2005; Ishidoya et al., 2006; Manning and Keeling, 2006).

To better understand the atmospheric oxygen cycle, the concept of atmospheric potential oxygen (APO) has been introduced. APO is expressed conceptually as $\mathrm{APO} = O_2 + 1.1 \times CO_2$ (Stephens et al., 1998), where 1.1 is the assumed globally averaged $-O_2$:CO_2 molar ratio for land biotic photosynthesis and respiration (Severinghaus, 1995). APO is invariant with respect to terrestrial biotic exchanges and only weakly dependent on fossil fuel combustion, which contributes to the observed long-term APO decrease. Thus temporal variations and global distributions of APO predominantly reflect variations in the oceanic exchange of O_2. Therefore, APO has been used, for example, in studies

*Corresponding author.
e-mail: tohjima@nies.go.jp
DOI: 10.1111/j.1600-0889.2007.00334.x

of ocean productivity (Keeling and Shertz, 1992; Bender et al., 1996; Balkanski et al., 1999), of air–sea gas exchange velocity for O_2 (Keeling et al., 1998b), and of large-scale ocean transport (Stephens et al., 1998; Gruber et al., 2001; Tohjima et al., 2005b; Battle et al., 2006). In addition to the above applications, Bender et al. (2005) and Manning and Keeling (2006) proposed a new method based on APO to solve the global oceanic and land biotic carbon sinks. Manning and Keeling (2006) showed that this APO approach, combined with the global CO_2 observation from the Global Monitoring Division of the National Oceanic and Atmospheric Administration's Earth System Research Laboratory (hereinafter abbreviated to NOAA/ESRL GMD, formally known as NOAA/CMDL), can provide more robust estimations of CO_2 sinks than the conventional approach based directly on the atmospheric O_2 change.

In this paper, we present atmospheric O_2/N_2, CO_2 and APO at Hateruma Island (HAT, lat 24°03′N, long 123°48′E) and Cape Ochi-ishi (COI, lat 43°10′N, long 145°30′E) in Japan. We also present some discussion about our O_2/N_2 reference scale and its stability. Using the APO from our stations, in conjunction with the NOAA/ESRL GMD globally averaged atmospheric CO_2 record, we present our estimates of the global carbon budget. We also discuss the effect of the oceanic O_2 outgassing and uncertainties associated with the global carbon budget. Finally, we examine the rate of change in the deseasonalized APO trends obtained at HAT and COI.

2. Experimental method

2.1. Definition of $\delta(O_2/N_2)$ and δAPO

Changes in O_2 concentration are expressed as relative deviations of the O_2/N_2 ratio from an arbitrary reference:

$$\delta(O_2/N_2) = [(O_2/N_2)_{\text{sample}}/(O_2/N_2)_{\text{reference}} - 1] \times 10^6. \quad (1)$$

Following Keeling and Shertz (1992), we use the units of 'per meg' to express the $\delta(O_2/N_2)$ value. A value of 4.8 per meg is equivalent to the same number of molecules as 1 μmol mol^{-1} (ppm) in a trace gas abundance. Here, the $\delta(O_2/N_2)$ values are determined against our original reference scale, the details of which are discussed in the following section.

We calculate δAPO according to

$$\delta\text{APO} = \delta(O_2/N_2) + \alpha_B X_{CO_2}/S_{O_2} - 1850, \quad (2)$$

where X_{CO_2} is the CO_2 mol fraction in ppm, α_B is the $-O_2$:CO_2 molar exchange ratio for the land biotic respiration and photosynthesis, S_{O_2} is the atmospheric O_2 mole fraction ($S_{O_2} = 0.2094$) that is required to convert units of ppm into per meg equivalent, and 1850 is an arbitrary APO reference point (1850 per meg). It should be noted that eq. (2) is a simplified version of the original definition of APO given by Stephens et al. (1998).

2.2. Outline of the flask sampling and analytical method

The air samples were collected in Pyrex glass flasks equipped with two glass stopcocks sealed by Viton® O-rings. We started monthly manual sampling at HAT by using 1-l flasks (six flask replicates per month) in July 1997 and 2-l flasks (four flask replicates per month) in February 1999, and automatic sampling at COI by using 2-l flasks in December 1998 (Tohjima et al., 2003). The sampling frequency for COI was two flasks per week (Monday and Friday), but this was changed to every 4 d after July 2004. In addition, we started automatic sampling at HAT in December 1999 with a sampling frequency of one flask every 4 d. Note that there are no replicates with the automated sampling.

The sampling pressure was 0.2 MPa (0.1 MPa above ambient pressure). The O_2/N_2 ratio of the pressurized air samples in our glass flasks decreased gradually during the storage period due to the preferential diffusion of O_2 through the Viton® O-ring (Sturm et al., 2004). The decrease rates were estimated to be about 0.4 per meg d^{-1} for the 1-l flasks and 0.2 per meg d^{-1} for the 2-l flasks (see Appendix). Therefore, corrections for the permeation effects for the individual storage periods were applied in this study. The average storage period from the sampling to the analysis for the manually collected samples was about 7 d, corresponding to a correction of 2.8 per meg for the 1-l flasks. Because the pressures upstream and downstream of the flasks connected to the automatic sampling system were kept close to the sampling pressure, the permeation effect would have been minimal while the flasks were connected to the automatic sampling system. Thus, we defined the period from the time when the flasks were removed from the automatic sampling system to the analysis as the storage period. The average storage period for the automatic sampling was about 8 d, corresponding to a correction of 1.6 per meg.

The collected air samples were sent back to our laboratory, and the O_2/N_2 ratios were measured with a gas chromatograph equipped with a thermal conductivity detector (GC/TCD) (Tohjima, 2000), while CO_2 mole fractions were measured by a non-dispersive infrared analyser (LiCor, LI-6252). The average standard deviations (1σ) of the flask replicates for O_2/N_2 and CO_2 measurements were about 8 per meg and 0.08 ppm for the 1-l flasks and 5 per meg and 0.05 ppm for the 2-l flasks (Tohjima et al., 2003).

2.3. NIES O_2/N_2 scale

2.3.1. Reference gases. We have used compressed air in high-pressure cylinders as reference gases for the O_2/N_2 ratio measurements. Sets of 47-l chrome-molybdenum steel cylinders filled with natural air (referred to as the HDA series), 48-l aluminum cylinders filled with natural air (referred to as the AT series), and 10-l and 48-l aluminum cylinders filled with purified air (referred to as the CPB and CQB series, respectively) were filled for this purpose by subcontractors. Hitachi Sanso Corp. (Hitachi, Japan) prepared the HDA and the AT series by

compressing the natural air at Kashima, Japan, after drying by charcoal trap, into cylinders. Japan Fine Products Corp. (Kawasaki, Japan) prepared the CPB and the CQB series by using purified natural air. The O_2/N_2 ratio of the purified air was several hundred per meg lower than the ambient level and the CO_2 concentration was less than 0.1 ppm because some parts of the purifying processes such as the oxidation of hydrocarbons on Pt catalyst and trapping of CO_2 and H_2O on a Molecular Sieve 5A could have altered the compositions. Therefore, the composition of the reference gases prepared from purified air was adjusted to ambient levels by adding pure CO_2 and O_2. Pressures during the initial filling of the cylinders were 13 MPa for the HDA and AT, 10 MPa for the CPB, and 8 MPa for CQB cylinders. The pressures in these cylinders during use did fall below about 2 MPa.

Following Keeling et al. (1998a, 2007), the reference cylinders were laid horizontally on a shelf covered by thermal insulation to minimize thermal and gravimetric fractionation effects. Each cylinder was connected to a regulator (Nissan Tanaka Corp., Japan, model ATR-203) by using an aluminum gasket, which effectively prevented the decrease in the O_2/N_2 ratio which has been observed to take place when polymeric gaskets are used. The flow rate of the gases delivered to our analytical system (8 cm^3 min^{-1}) was lower than the rate (300 cm^3 min^{-1}) adopted for the interferometric system by Keeling et al. (1998a). Recently, Keeling et al. (2007) suggested that the fractionation of the O_2/N_2 ratio at the regulator orifice might not be negligible when the flow rate of the gas is relatively low. However, we have not observed any change in the O_2/N_2 ratio of the remaining air in the cylinder with the pressure decrease (Tohjima et al., 2005a). Therefore, we concluded that the fractionation effect of the regulator is insignificant with our analytical conditions. The head valves used on all of our reference cylinders are sealed with Teflon tape, not Viton® O-rings, at the head valve base. Therefore, influence of the permeation of O_2 through the valve sealant, which causes a persistent decrease in the O_2/N_2 ratio when Viton® O-rings are used as the valve sealant (Keeling et al., 2007), is considered to be negligible for our reference cylinders.

2.3.2. Development of the NIES O_2/N_2 scale. During the first period (1997–2001) of the O_2/N_2 measurements, we used only three reference cylinders and the reliability of the reference scale depended on the stability of the O_2/N_2 ratio in those cylinders. After 2001 (in the second period), we increased the number of reference gases to assess the stability of our reference scale more precisely. The NIES scale is based on the initial composition of the air in HDA-1, as described by Tohjima (2000), and all other cylinders are referenced to it. Each cylinder with its identification number, its purpose, the value of $\delta(O_2/N_2)$, and the time of use are summarized in Table 1. Below, we describe the calibration procedure for the working references, as well as the determination and stability of our reference scale.

Table 1. List of cylinders used for primary and working references of O_2/N_2 measurements

Cylinder no.	Purpose	$\delta(O_2/N_2)$ (per meg)	Dates of use
HDA-1	Primary and working	0	Jul. 1997–Sep. 1999
HDA-2	Primary	−57	Jul. 1997–Jun. 2001
HDA-4	Primary and Working	−125	Sep. 1999–Jun. 2002
CPB10227	Primary	−176	Jun. 2001-
CPB10228	Primary	−181	Jun. 2001-
CPB26028	Primary	−113	Jun. 2001
CPB26029	Primary	−172	Jun. 2001
CPB26030	Primary	−211	Jun. 2001
CQB07071	Primary	−442	Aug. 2001-
CQB07072	Primary	−232	Aug. 2001-
CQB07074	Primary	−175	Aug. 2001-
CQB12690	Primary	−204	Dec. 2001-
CQB12691	Primary	−234	Dec. 2001-
CQB12692	Primary	−227	Dec. 2001-
AT-1	Primary	−493 ∼ −525	Jul. 2001–Aug. 2002
AT-2	Primary	−371 ∼ −384	Jul. 2001–Oct. 2001
AT-3	Primary	−110 ∼ −152	Jul. 2001–Dec. 2001
AT-4	Working	−113 ∼ −208	Jun. 2001–Mar. 2002
CQB12693	Working	−204	Mar. 2002–Dec. 2002
CQB07076	Working	−195	Dec. 2002–Dec. 2003
CQB15647	Working	−191	Dec. 2003–Nov. 2004
CQB16960	Working	−198	Nov. 2004–Mar. 2006

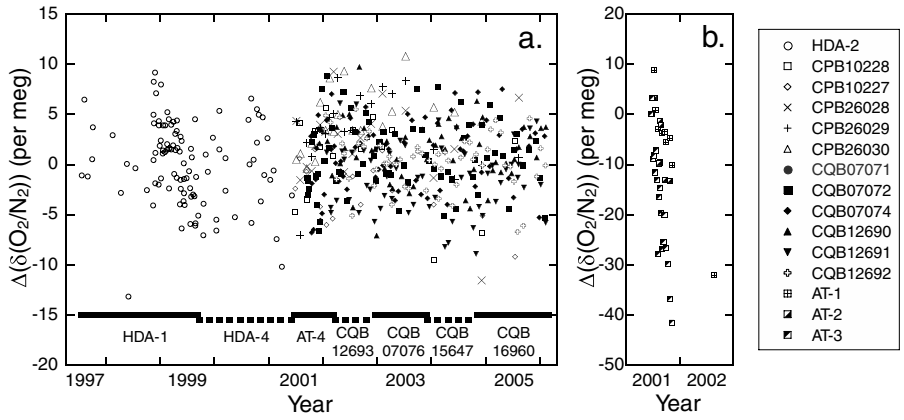

Fig. 1. (a) History of the O_2/N_2 ratios of the 12 cylinders relative to the NIES scale. In the first period (1997–2001) the changes in the $\delta(O_2/N_2)$ values from the average of HDA-2 are plotted. In the second period (2001–2006) the changes in the $\delta(O_2/N_2)$ values from the initial values of the 11 reference cylinders are plotted. Each horizontal bar indicates the period of time when each working reference gas was used. (b) Rapid decreases in the O_2/N_2 ratio of the three cylinders (AT-1, AT-2, and AT-3) relative to the NIES scale. These cylinders were removed from the set of primary reference gases.

Initially, the cylinder HDA-1 was also used as a working reference during the period from July 1997 to September 1999. A 2nd working gas (HDA-4), the O_2/N_2 ratio of which was directly determined against HDA-1, was used during the period from September 1999 to July 2001. We compared these working gases frequently with another high-pressure cylinder (HDA-2) to evaluate the stability of the O_2/N_2 reference scale. The temporal changes in the HDA-2 O_2/N_2 ratio against the other two reference gases are shown in Fig. 1a; plotted values are the residuals from the average. The period of time when each working reference gas was used is also shown in Fig. 1a as a horizontal bar with the cylinder ID. The rate of drift, or the drift rate, of HDA-2 relative to the HDA-1 and HDA-4 during the first period, determined by the least square fitting, was –0.1 $\pm$ 0.2 per meg yr^{-1}.

In 2001 (the end of the first period), the O_2/N_2 ratios of the five 10-l cylinders (CPB series) and the six 47-l cylinders (CQB series) were carefully determined against the HDA-1 scale. The O_2/N_2 ratios of these references ranged from -450 to -100 per meg on the NIES scale. In the second period, these reference cylinders were used as primary reference gases. The working reference gases were periodically compared against these primary reference cylinders during the period of use. We did not find any significant O_2/N_2 drifts in the working reference cylinders except in cylinder AT-4. Thus, at the end of the usage of the reference gas, we have adopted an average of the individual O_2/N_2 ratios against the primary reference cylinders as the O_2/N_2 ratio for each working reference. In this way, the NIES O_2/N_2 scale is propagated. The temporal changes in the O_2/N_2 ratios of the 11 primary reference cylinders and three AT cylinders against the NIES scale in the second period of observation are also shown in Fig. 1a and b, respectively, in which the residuals from the initially determined values are plotted. Figure 1b shows that the cylinders AT-1, AT-2 and AT-3 display rapid decreases in the O_2/N_2 ratios. Thus we did not use these cylinders as primary references. Unfortunately one cylinder AT-4 was used as a working reference gas during the period from June 2001 to March 2002, also showing rapid decrease in the O_2/N_2 ratio. The drift rate of about -80 per meg yr^{-1} for the cylinder AT-4 was almost constant during the 270-d period of its usage. Therefore, we adopted a linearly drifting O_2/N_2 ratio for AT-4. This procedure sufficiently removed the error associated with the O_2/N_2 change in this particular reference gas. The nominal dew point for HDA and AT series was less than -40 °C while the nominal dew point for CPB and CQB series was less than -80 °C. Thus, we hypothesize that the rapid decreases in the O_2/N_2 ratio for the cylinders of the AT series were caused by oxidation of the interior surface of the cylinder, which could have been enhanced by insufficient drying. The difference in the oxidative activity of the interior surface between HDA and AT series might be explained by the fact that the HDA cylinders were old and had been repeatedly filled with dry air while the AT cylinders were new and were filled with dry air for the first time in this study.

Drift rates of the reference cylinders during the second period (about 4 yr long), determined by least square fitting with a straight line, ranged from -0.8 to 0.6 per meg yr^{-1}, with a standard deviation of 0.5 per meg yr^{-1}. It is difficult to evaluate the absolute drift rate of our reference scale, because we have not succeeded in developing absolute O_2/N_2 standards or absolute analytical methods with sufficient precision. Recently, Tohjima et al. (2005a) prepared a standard mixture composed of CO_2, Ar, O_2 and N_2 by gravimetric technique, and achieved a precision of about 16 per meg. However, the precision is not good enough to evaluate the exact drift rate of the O_2/N_2 ratio during the period of our study. Accordingly, in this study, we have assumed that

the absolute drift rate during the second period was within twice the standard deviation of the drift rate of the reference cylinders, that is, the uncertainty of the stability of NIES O_2/N_2 scale was assumed to be ± 1 per meg yr^{-1}. We also adopted the value of this uncertainty for the uncertainty in the NIES scale during the first period. Consequently, the estimate of the uncertainty in the NIES scale for the whole period was ± 1 per meg yr^{-1}.

2.4. Equations for land-ocean carbon sink partitioning

The terms and equations used in atmospheric O_2 studies have been described in detail by Manning and Keeling (2006). Here, we summarize the equations required to compute the oceanic and land biotic carbon sinks. The global mass balances of atmospheric CO_2 and O_2 are expressed by

$$\Delta X_{CO_2} = \beta \times (\mathrm{F} - \mathrm{O} - \mathrm{B}), \text{ and} \tag{3}$$

$$\Delta[\delta(O_2/N_2)] = (\beta/S_{O_2}) \times (-\alpha_F \mathrm{F} + \alpha_B \mathrm{B} + Z_{eff}), \tag{4}$$

where

$$\beta = 10^{21}/(m_c \times n_{air}), \tag{5}$$

where ΔX_{CO_2} is the change in the atmospheric CO_2 mole fraction expressed in units of ppm yr^{-1} and $\Delta[\delta(O_2/N_2)]$ is the change in the $\delta(O_2/N_2)$ ratio in units of per meg yr^{-1}. F is the CO_2 emission from fossil fuel burning and cement manufacturing, O is the ocean CO_2 uptake, and B is the land biotic CO_2 uptake. F, O and B are given in units of Pg C yr^{-1}. m_c represents the molecular mass of carbon, taken as 12.01 g, n_{air} is the total number of moles of dry air and β is the coefficient converting Pg C to ppm CO_2. α_F is the globally averaged $-O_2$:CO_2 molar exchange ratio for fossil fuel burning. The constants used in these equations are summarized in Table 2. Z_{eff} is the net effect of oceanic outgassing of O_2 and N_2 on the atmospheric O_2/N_2 ratio, given in units of Pg C yr^{-1}. Manning and Keeling (2006) gave the expression of Z_{eff} as

$$Z_{eff} = \left(Z_{O_2} - Z_{N_2}\frac{S_{O_2}}{S_{N_2}}\right) \times m_c \times 10^{-15}, \tag{6}$$

where Z_{O_2} and Z_{N_2} represent the net oceanic fluxes of O_2 and N_2 in units of mol yr^{-1}, respectively (positive means flux to the atmosphere) and S_{N_2} is the atmospheric N_2 mole fraction.

Solving eqs (3) and (4) for O and B, and substituting eq. (2) into the solutions, we obtain

$$O = \left[-(\alpha_F - \alpha_B)\,F - \left(\frac{S_{O_2}}{\beta}\right) \times \Delta(\delta\mathrm{APO}) + Z_{eff}\right] \times \frac{1}{\alpha_B}, \tag{7}$$

and

$$B = \left[\alpha_F F + \left(\frac{S_{O_2}}{\beta}\right) \times \Delta(\delta\mathrm{APO}) - \left(\frac{\alpha_B}{\beta}\right) \times \Delta X_{CO_2} - Z_{eff}\right] \times \frac{1}{\alpha_B}. \tag{8}$$

In this study, we have calculated oceanic and land biotic carbon sinks by using eqs (7) and (8). As was done in Manning and Keeling (2006), we have used the global CO_2 data from the NOAA/ESRL GMD network for the atmospheric CO_2 change in eq. (8).

Table 2. Values of coefficients for calculating the fossil fuel CO_2 sinks

Symbol	Description	Value
S_{O_2}	Atmospheric O_2 mole fraction	0.2094[a]
S_{N_2}	Atmospheric N_2 mole fraction	0.7809[a]
m_c	Atomic mass of C (g $mole^{-1}$)	12.01
n_{air}	Total number of moles of dry air	1.773×10^{20}[b]
α_B	Land biotic $-O_2$:C molar exchange ratio	1.10[c]
β	Unit conversion coefficient (Pg C to ppm)	0.470[d]

[a]Recently revised value from Tohjima et al. (2005a).
[b]Based on the total mass of dry air of 5.1352×10^{21} g (Trenberth and Smith, 2005) and mean molecular weight of dry air of 28.965 g (Tohjima et al., 2005a).
[c]From Severinghaus (1995).
[d]Calculated from eq. (5).

3. Results and discussion

3.1. Calculation of long-term changes in O_2/N_2 and APO observed at HAT and COI

Observed O_2/N_2, CO_2 and APO at HAT and COI are shown in Fig. 2, together with the corresponding smooth curves fitted to the data. When more than two samples are collected on the same day, the averaged value is plotted. We fit the curves following the methods of Thoning et al. (1989) with a cut-off frequency of 4.6 cycles yr^{-1}. This is roughly equivalent to a 40-d running average.

We have calculated the annual means by using a similar procedure to that adopted by Keeling et al. (1996). We first calculate the monthly means from the observed data that are adjusted to the 15th of individual month by shifting them parallel to the smooth-curve fits, and then calculate the annual mean from the consecutive 12 monthly means. There are no data at HAT in November 1998, so the 15th data of the smooth-curve fit is used toward the calculation of the 1998 annual mean. We calculate annual means in two ways: one from the smooth-curves and the other following Keeling et al. (1996). Results differ by less than ± 1 per meg (rms).

Figure 3 shows the residuals of individual APO from the respective smooth-curve fit at HAT and COI. The residuals of APO at HAT are less scattered before December 1999. This reflects the fact that before December 1999 each point represents an average of five flasks (three 1-l flasks and two 2-l flasks) and that the smooth-curve follows the data more closely due to the longer sampling interval (monthly sampling). The uncertainties

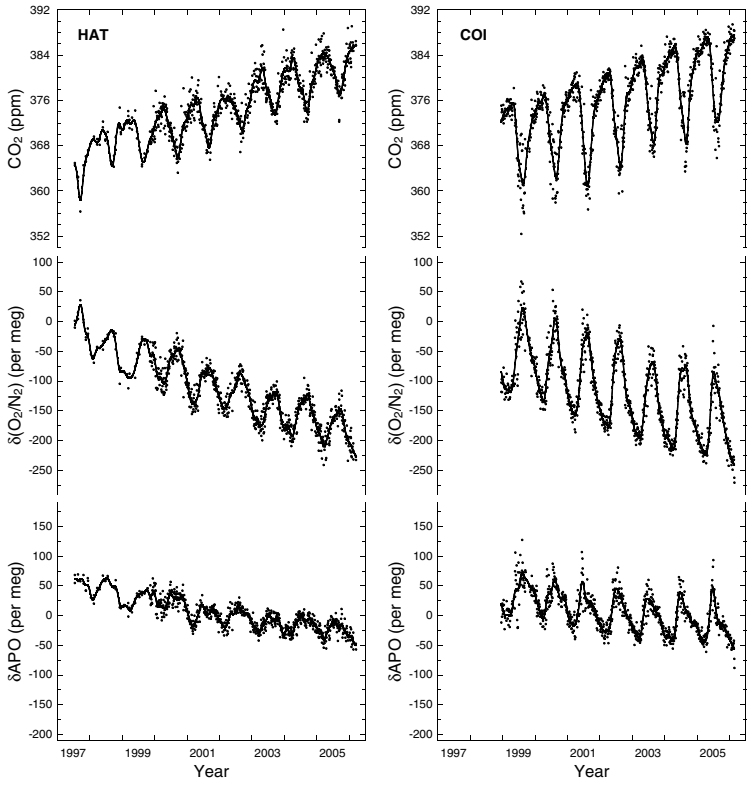

Fig. 2. Time series of observed (a) CO_2 mole fraction, (b) O_2/N_2 ratio, and (c) APO at HAT (left-hand panel) and COI (right-hand panel). The *y* axes have been scaled so that the $\delta(O_2/N_2)$ and δAPO variations shown are two times larger than the CO_2 variations shown on a molar basis. Each point is the average of replicate flasks collected at the same day. Solid lines indicate the smooth-curve fits (details are described in the text).

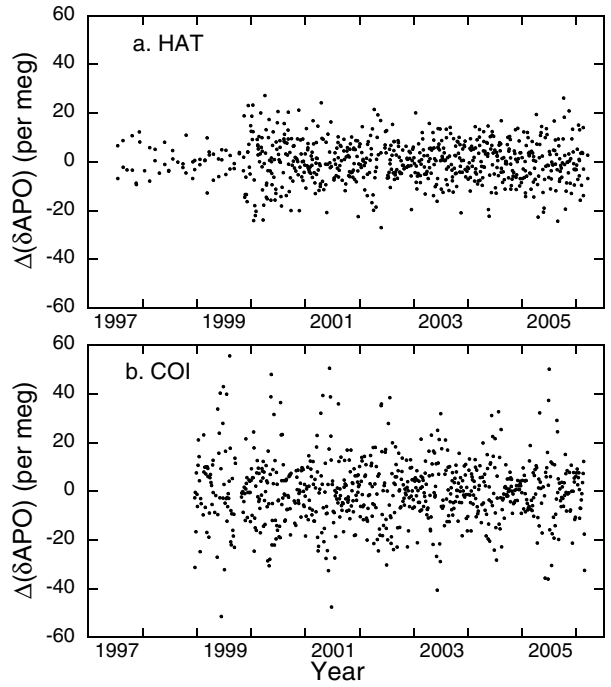

Fig. 3. Residuals of the observed APO from the smooth-curve fits for (a) HAT and (b) COI.

associated with the determination of the annual mean APO are calculated as the standard errors of the residuals. For example, the standard errors for HAT are 1.0 per meg ($n = 21$) for the 1-yr period centred on 1 July 1998 and 0.92 per meg ($n = 105$) for the 1-yr period centred on 1 July 2005; those for COI are 2.1 per meg ($n = 93$) for the 1-yr period centred on 1 July 1999 and 1.35 per meg ($n = 97$) for the 1-yr period centred on 1 July 2005.

3.2. Estimation of the ocean outgassing effect

Upper-ocean warming is expected to affect the sea-to-air O_2 exchange in several ways. For example, increases in seawater temperature would reduce the solubility of O_2, resulting in an increase in oceanic O_2 outgassing. Upper-ocean warming would also strengthen the vertical stratification, causing a reduction in the convective outcropping of the O_2-depleted deep water. This would result in a reduction of the oceanic O_2 drawdown during winter, lowering the oceanic O_2 inventory. Several studies have already been devoted to the estimation of the oceanic O_2 outgassing effect caused by global warming (Bopp et al., 2002; Keeling and Garcia, 2002; Plattner et al., 2002). In those studies, the net oceanic O_2 fluxes were computed as a product of two estimates: oceanic O_2 flux-to-heat flux ratio and the net ocean heat flux. Modest differences in the estimates of the O_2 flux-to-heat flux ratio, ranging from 5 to 6 nmol J^{-1}, have been noted. But the estimates of the net ocean heat flux, based on the observed

oceanic heat content of Levitus et al. (2000), showed rather large differences, resulting in large discrepancies in the estimates of the carbon flux, ranging from 0.3 to 0.8 Pg C yr^{-1}. The large differences in the ocean heat flux estimate may be ascribed to the differences in the ocean model used to extrapolate the ocean heat flux. Manning and Keeling (2006) adopted a new estimate of the oceanic heat flux of 9.2×10^{22} J for the period between 1993 and 2003 that was computed from the combined data of satellite altimetric height and in situ temperature profiles by Willis et al. (2004). With this new oceanic heat flux value, they obtained a correction value for the carbon sequestration ($Z_{\rm eff}$) of 0.48 Pg C yr^{-1} by using the oceanic O_2 flux-to-heat flux ratio of Keeling and Garcia (2002) and eq. (6).

Recently, Lyman et al. (2006) reported a rapid cooling of 3.2×10^{22} J in the upper (0–750 m) ocean between 2003 and 2005 by using a broad array of in situ temperature data. However, more recently, this rapid cooling was found to be an artefact that was caused mainly by an error in the calibration of a subset of Argo floats (Schiermeier, 2007). Lombard et al. (2007), comparing satellite altimetric height data with satellite gravity data, showed that the thermosteric sea level increased between August 2002 and April 2006 and that the increase rate was consistent with the thermal expansion rate of the sea level based on the global ocean temperature data between 1998 and mid-2003. Their results appear to suggest that the ocean heat content steadily increased over the period from 1998 to 2006. The heating rate of Willis et al. (2004) for the period 1998–2003 is close to that for the 10-yr period from 1993 to 2003 because of a slow warming observed during 1993–1996 and a rapid warming during 1996–1998 (see fig. 3 of Willis et al., 2004). Therefore, we adopt the heating rate of 9.2×10^{21} J yr^{-1}, which is exactly the value Manning and Keeling (2006) adopted, for our observation period (1998–2005). We also adopt the same approach in calculating the correction value for the carbon sequestration ($Z_{\rm eff}$) as Manning and Keeling (2006), and consequently obtain the exact same correction value of 0.48 Pg C yr^{-1}. In the above calculations, it is assumed that the O_2-to-heat flux ratio is constant. However, Garcia et al. (2005) examined the temporal variations in O_2 and heat content in the top 100 m of the world ocean between 1955 and 1998, and found that the O_2-to-heat flux ratio varies substantially depending on the decadal periods. Thus the O_2 flux estimation based on the recent ocean heating rate may still have a large error. Here, we assume an uncertainty of 100%, or 0.48 Pg C yr^{-1}.

3.3. Calculation of global carbon budgets

We calculate the partitioning of the global carbon sink for the 7-yr period from 1 July 1998 to 1 July 2005 based on the APO data from HAT, and for the 6-yr period from 1 July 1999 to 1 July 2005 based on the data from HAT and COI. Following the method of Manning and Keeling (2006), we subtract the annual average of the endpoint from the annual average of the beginning point to obtain ΔAPO. The fossil fuel emission rate for the period 1998–2003 is obtained from Marland et al. (2006) and extrapolated to 2004 and 2005. Using the $-O_2$:C molar exchange ratio for each fuel type given by Keeling (1988), we calculate the average $-O_2$:C exchange ratios for the fossil carbon emission ($\alpha_{\rm F}$). In these calculations, we assume 1.40 for $\alpha_{\rm F}$ for 2004 and 2005 because the average and standard deviation (1σ) of $\alpha_{\rm F}$ for 1998–2003 is 1.40 ± 0.01. Globally averaged monthly mean atmospheric CO_2 data are obtained from the marine surface sites of the NOAA/ESRL GMD flask sampling network (http://www.cmdl.noaa.gov/ccgg/trends/) (P. Tans and T. Conway, personal communication, 2007). For our study, we use the ocean outgassing correction value of 0.48 PgC yr^{-1}, as discussed in Section 3.2. The resultant estimates of the oceanic and land biotic carbon sinks, together with the values used in the individual calculations, are summarized in Table 3. The uncertainties associated with the estimated sinks, which are discussed in the following section, are also listed in the table.

The oceanic and land biotic carbon sinks for the full 7-yr period of our study, evaluated from our longest record at HAT, are 2.4 and 0.5 Pg C yr^{-1}, respectively. For the later 6-yr period of our study, we obtain oceanic and land biotic sinks of 2.1 and 1.0 Pg C yr^{-1}, respectively, by averaging the APO records from HAT and COI. We also compute the land and ocean sinks for the 6-yr period using the APO data from HAT and COI separately (Table 3), and find the differences to be less than 0.1 Pg C yr^{-1}, showing the similarity of the APO change observed at HAT and COI. On the other hand, the HAT data point to a decrease in the oceanic sink of 0.4 Pg C yr^{-1} and an increase in the land biotic sink of 0.5 Pg C yr^{-1} from the first period to the second period. As discussed in Section 3.5, there are large interannual variations in the APO trends, causing the estimation of carbon sinks to be sensitive to the time period of interest.

We also list the recent estimates of the oceanic and land biotic CO_2 sinks based on the APO measurements of Bender et al. (2005) and Manning and Keeling (2006) in Table 3. For a more consistent comparison, we recalculate their estimates by using the updated global CO_2 change from the NOAA/ESRL GMD data, the updated fossil fuel statistics, and the ocean O_2 outgassing correction ($Z_{\rm eff}$) of 0.48 Pg C yr^{-1}. Our estimates of the oceanic and land biotic CO_2 sinks agree with their estimates within the uncertainties, but our land biotic sinks for the later 6-yr period are larger by about 0.4 Pg C yr^{-1}. The differences between the estimates of the other studies and ours are due mainly to the different periods for which the sinks are calculated. This is important because the APO and CO_2 trends are time sensitive (Manning and Keeling, 2006).

3.4. Uncertainty in the carbon budgets

The uncertainties in the parameters in eqs (7) and (8) used to calculate carbon sequestration are summarized in Table 4, which contains exactly the same information in the same format as table

Table 3. Fossil carbon sequestration rates based on the O_2/N_2 observation from this work and other recent works

Time period	Stations	ΔAPO (per meg yr^{-1})	ΔCO_2[a] (ppm yr^{-1})	F[b] (Pg C yr^{-1})	α_F[c] (mol mol^{-1})	Z_{eff}[d] (Pg C yr^{-1})	Ocean sink (Pg C yr^{-1})	Land sink (Pg C yr^{-1}) (Pg C yr^{-1})
This study								
1998.5–2005.5	HAT	−9.49	1.90	6.94	1.396	0.48	2.41 ± 0.7	0.49 ± 0.9
1999.5–2005.5	HAT	−8.65	1.87	7.00	1.395	0.48	2.06 ± 0.7	0.96 ± 0.9
1999.5–2005.5	COI	−8.62	1.87	7.00	1.395	0.48	2.05 ± 0.7	0.97 ± 0.9
1999.5–2005.5	HAT, COI	−8.64	1.87	7.00	1.395	0.48	2.06 ± 0.7	0.96 ± 0.9
Bender et al. (2005)								
1993.5–2002.5	CGO	−8.90[e]	1.76	6.57	1.397	0.48	2.27 ± 0.5[f]	0.57 ± 0.6[f]
Manning and Keeling (2006)								
1993.0–2003.0	ALT, LJO, CGO	−8.78	1.75	6.57	1.397	0.48	2.22 ± 0.6[f]	0.62 ± 0.7[f]

[a]Based on global CO_2 data from the NOAA/CMDL network.
[b]Based on global CO_2 production data from fossil fuel burning and cement manufacturing (Marland et al., 2006) and some extrapolated data.
[c]Calculated from CO_2 production figures by fossil fuel types (Marland et al., 2006) and the O_2:C molar combustion ratios for individual fuel types (Keeling, 1988).
[d]The values of Z_{eff} are calculated by using eq. (6), the ocean heating rate of Willis et al. (2004) and the oceanic O_2 and N_2 flux/heat flux ratios of Keeling and Garcia (2002).
[e]Bender et al. (2005) did not explicitly give the value of $\Delta(\delta O_2/N_2)$ or ΔAPO. The value listed here is calculated from the atmospheric CO_2 increase rate at CGO, fossil fuel CO_2 production, O_2:C combustion ratio, and oceanic CO_2 sink given by Bender et al. (2005).
[f]These values are different from the published values because revised values listed here (except ΔAPO) are used. The original oceanic and land sinks are 1.8 and 1.1 Pg C yr^{-1} for Bender et al. (2005) and 2.24 and 0.51 Pg C yr^{-1} for Manning and Keeling (2006).

Table 4. Estimates of uncertainties in the parameters used to calculate oceanic and land biotic CO_2 sequestrations for the 6-yr period (1999.5–2005.5)

Parameter	Uncertainty	Oceanic sink (Pg C yr^{-1})	Land sink (Pg C yr^{-1})
Fossil fuel emission	0.4 Pg C yr^{-1}	0.11	0.53
Z_{eff}	0.48 Pg C yr^{-1}	0.44	0.44
α_B	0.05	0.05	0.05
α_F	0.04	0.25	0.25
ΔAPO (synoptic variability)	0.41 per meg yr^{-1}	0.17	0.17
ΔAPO (drift of the scale)	1.0 per meg yr^{-1}	0.40	0.40
ΔAPO (site difference)	0.2 per meg yr^{-1}	0.08	0.08
ΔCO_2	0.02 ppm yr^{-1}	0	0.04
Square root of the square sum		0.68	0.86

5 in Manning and Keeling (2006), except for the results from this study. As for the uncertainty associated with the fossil fuel burning statistics, we use ±6% of the CO_2 emission (Marland and Rotty, 1984). The uncertainty of ±0.05 in α_B is derived from the study of Severinghaus (1995). We estimate the uncertainty in α_F from uncertainties associated with the individual O_2:CO_2 combustion ratios for 4 different fuel types (e.g. coal, liquid, natural gas and gas flaring) (Keeling, 1988) and ±6% uncertainties in the individual emissions, which are assumed to be independent of each other. The contributions of the former and latter uncertainties in α_F are ±0.02 and ±0.03, respectively, and the overall uncertainty in α_F is evaluated as a square root of the squared sum to be ±0.04. Global atmospheric CO_2 measurements have uncertainty of less than 0.1 ppm (Conway et al., 1994), which corresponds to an uncertainty in the change rate of global mean CO_2 of about 0.02 ppm yr^{-1}.

The uncertainties in the APO change arise from several factors, including (1) the uncertainty in the annual mean APO caused by the analytical errors and synoptic variability, (2) the drift in the reference scales of APO and (3) the uncertainty in the global trend due to the limited number of observation sites. Taking into account the uncertainties associated with the calculation of the annual mean APO, as discussed in Section 3.1, we obtain the contribution of factor (1) of 0.19 per meg yr^{-1} at HAT for the 7-yr period and 0.42 per meg yr^{-1} at COI for the 6-yr period. The stability of the reference scale of APO depends acutely on the stability of the O_2/N_2 reference scale because the CO_2 reference scale has been kept relatively constant within 0.1 ppm for

the observation period. The stability of our CO_2 scale was confirmed by the results of the WMO Round-robin intercomparison program conducted in 1995–1997, 1999–2000 and 2002–2005. Therefore, the contribution of factor (2) to the uncertainty in the APO change is ± 1 per meg yr^{-1}, as discussed in Section 2.3.2. It is difficult to evaluate the uncertainty caused by the limited observation [factor (3)]. However, we adopt the value of 0.2 per meg yr^{-1} used by Manning and Keeling (2006). They evaluated the uncertainty as a range of different APO trends obtained by changing the site selection. They included at least one site from each hemisphere for the site selection, but our sites are both located in the Northern Hemisphere. Therefore, it is reasonable to assume that the value of 0.2 per meg yr^{-1} is probably the lower limit for our study.

Individual contributions to the uncertainties in the oceanic or land biotic sinks for the 6-yr period are summarized in Table 4. The dominant sources of error are the uncertainties in the oceanic outgassing correction, the observed APO change, and, in the case of the land biotic sink, fossil fuel emissions. The overall uncertainties in the oceanic and land biotic sinks, calculated as the square root of the sum of the squares of the individual contributions, are 0.7 and 0.9 Pg C yr^{-1}, respectively. Note that the uncertainties in the estimates for the 7-yr period are similar to these values. These uncertainties in our estimates are larger than those published in the recent studies by Bender et al. (2005) and Manning and Keeling (2006) (see Table 3) because the stability of our reference scale is less certain than theirs.

3.5. Interannual variation in APO

The instantaneous rate of change in APO for HAT and COI, calculated as the derivative of the deseasonalized trend, is shown in Fig. 4. The deseasonalized trends are computed as follows. First, the APO data are fitted with a function consisting of a linear trend and the sum of the first four harmonics of the annual cycle. The residuals from the fitted curve are averaged into monthly means which are then smoothed by a digital filtering technique (Thoning et al., 1989) with a cut-off frequency of 0.6 cycles yr^{-1} that corresponds to a wavelength of 20 months, a value similar to that used by Bender et al. (2005). The deseasonalized trend curve is, therefore, composed of two components: the averaged linear decreasing trend and the smoothed interannual fluctuation (from the digital curve fitting) around the linear trend. The instantaneous rate of change shown in Fig. 4 is therefore calculated as the derivative of the deseasonalized trend curve.

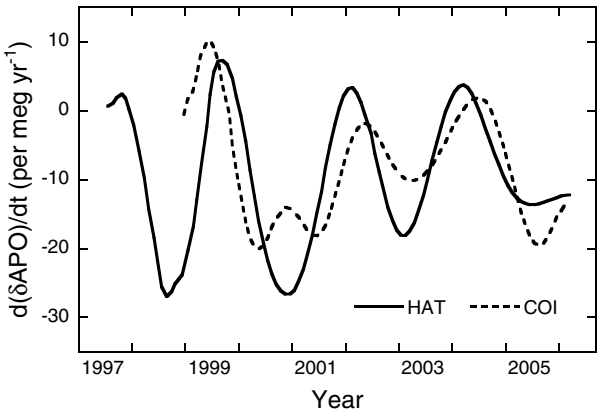

Fig. 4. Rates of change in the deseasonalized trends of APO at HAT (solid line) and COI (broken line).

The rates of change in APO at both sites show large variability, reflecting changes in the oceanic CO_2 or O_2 exchanges with the atmosphere. The interannual variability in the peak-to-peak amplitude of the rate of change reaches more than 30 per meg yr^{-1} at both sites. This variability, compared with the six global sampling sites reported in Bender et al. (2005), is much larger than the variability at Cape Grim, Barrow, Syowa and Samoa, but is comparable to the variability observed at Amsterdam Island and Macquarie Island. Assuming that the net oceanic O_2 flux is zero, that is $Z_{\mathrm{eff}} = 0$, the change rate in APO of 30 per meg yr^{-1} corresponds to a change in the oceanic uptake of 12 Pg C yr^{-1}. The atmospheric inverse model studies and ocean model studies showed much smaller variability in the oceanic CO_2 fluxes for the decadal period of 1990s. For example, variability estimated by the biogeochemical ocean GCM studies of Le Quéré et al. (2003) and McKinley et al. (2004) was less than 1 Pg C yr^{-1}. Patra et al. (2005) compared five atmospheric inverse model studies and found that the oceanic variability ranged from 1 to 4 Pg C yr^{-1}. From the results of these model studies, we conclude that much of the APO change observed at our sites is due to variability in the air–sea O_2 flux.

The rates of change in APO at HAT and COI are fairly consistent and roughly in phase with a range of lag from -6 to $+6$ months. The APO variations for the six sites examined by Bender et al. (2005) also exhibited similar phasing with each other. It is noteworthy, however, that the variations in APO at our sites seem to be out of phase with the sites studied by the Princeton group. The rates of change at HAT and COI (Fig. 4) show troughs around late 1998 and 2000, and peaks around late 1999. While the results of the Princeton group (fig. 6 of Bender et al., 2005) generally showed peaks around late 1998 and late 2000, and troughs around late 1999 and early 2002. Our sites are expected to be affected predominantly by the air–sea O_2 fluxes from the western North Pacific, while the sites of the Princeton group are located in the Southern Hemisphere (except Barrow). The differences in the phasing of APO between the two groups might reflect the regional differences in the temporal variability of the air–sea O_2 flux. Here, it should be noted that we cannot rule out the possibility that the drift in our standard scale could have contributed to the synchronous changes in the APO trends at our sites.

The interannual variability in APO is caused by the imbalance between the summertime O_2 emission associated with primary production in the ocean surface and the wintertime O_2 drawdown

associated with convection (Keeling et al., 1993; Bender et al., 1996). Seasonality in sea surface temperature (SST) enhances the above-mentioned seasonal O_2 fluxes through solubility forcing, and thus the interannual variability in SST could also contribute to the imbalance in the oceanic O_2 flux. Bopp et al. (2002), using a coupled climate-ocean biogeochemistry model, showed that the annual imbalances in the air–sea O_2 exchange are large in the regions of high biological productivity and intense vertical mixing, such as the equatorial Pacific, North Pacific, North Atlantic and Southern Ocean. The observed APO at COI shows large seasonality (Fig. 2) with larger variability during summer than in other seasons (Fig. 3). Recently, we started in situ measurements of the atmospheric O_2/N_2 ratio at COI by using a GC/TCD system, and have observed events with significantly variable and elevated APO during the period from April to July, corresponding to the times of intensive bloom events in the Sea of Okhotsk and the Pacific Ocean off the east coast of Hokkaido Island (H. Yamagishi, personal communication, 2007). These results suggest that the O_2 emissions associated with marine photosynthesis can cause the large variability in APO seen at COI, and could contribute to the interannual variability in APO.

In order to separately assess the influences of O_2 production during summer and O_2 drawdown during winter on the APO interannual variations, we decompose the rate of change into winter (October–March) and summer (April–September) components. Each component is computed in almost the same way as the rate of change was calculated before, except this time we set the monthly residuals in the opposing season to zero and remove the linear decreasing trends. Summer and winter rates of change in APO are depicted in Fig. 5a and b, respectively. It should be noted that, for each station, the sum of the summer and winter components is equivalent to the original rate of change shown in Fig. 4 except for the offset of the linear decreasing rate. For COI, the variability in the summer component is substantially smaller and the winter component is the one that mainly contributes to the interannual variation. For HAT, the summer and winter components contribute almost equally to the interannual variation. Back trajectory analysis indicates that the air masses arriving at HAT are predominantly transported from the north and south of the station in winter and summer, respectively, while the air masses arriving at COI are generally from the northwest in winter and from the southeast in summer but the seasonality is not as clearly defined as the one at HAT (Tohjima et al., 2002). Such transport generally means that the measurements at HAT are influenced by air masses from the mid-latitude regions in winter and from the low-latitude regions in summer, while the measurements at COI represent air masses from the mid-latitude regions all year around. Comparing the winter components of HAT and COI, we find excellent agreement, both in magnitude and phase (Fig. 5b). This agreement suggests that the interannual variability in the winter trend may be representative of the regional variability around Japan, perhaps of the western North Pacific as a whole. Above results suggest that the wintertime drawdown of

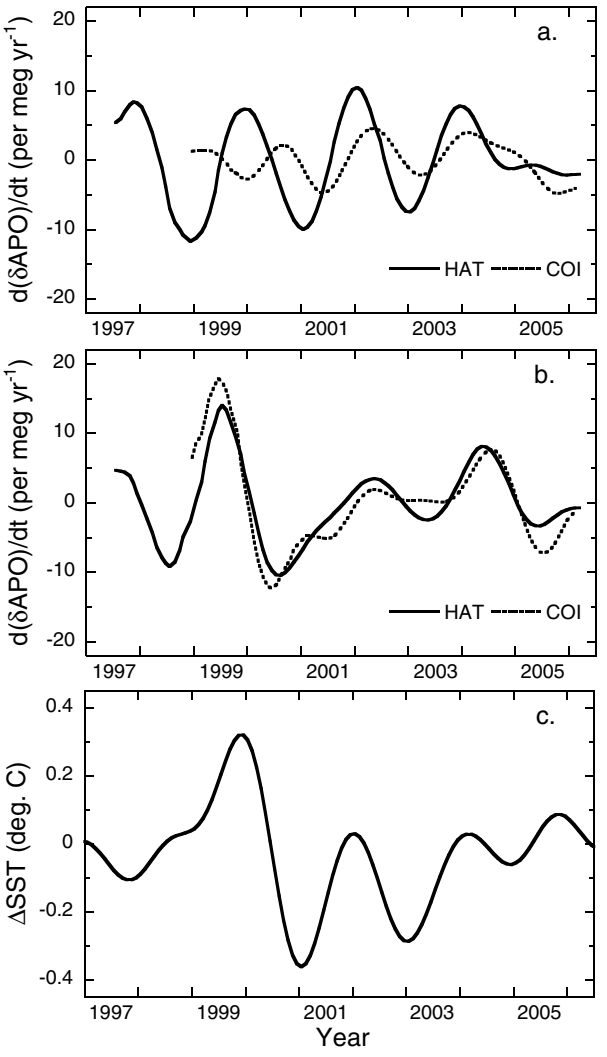

Fig. 5. Rates of change in the atmospheric APO calculated from (a) summertime anomaly and (b) wintertime anomaly. Solid line for HAT and broken line for COI. (c) Temporal changes in winter (October–March) SST anomaly in the rectangular region (36–50°N, 144–180°E) of the western North Pacific.

O_2 driven by vertical mixing is the main contributor to the interannual variability in APO at mid-latitude regions around the western North Pacific.

Recently, it has been shown that the Northern Hemisphere stations in the Scripps Atmospheric Oxygen Flask Sampling Network recorded sharp decreases in APO during the period from 1999 to early 2001 (R. Hamme, personal communication, 2007). These sharp decreases in APO have been attributed to the particularly cold SST in the northwestern North Pacific in the winter of 2000 and 2001, causing more vigorous ventilation and large drawdown of O_2. Our observations also show large decreases in the rates of change in APO both at HAT and COI during

2000–2001. In Fig. 5c, we depict the winter (October–March) component of monthly sea surface temperature (SST) anomaly for a rectangular region (36–50°N, 144–180°E) in the western North Pacific. The monthly SST data are obtained from the NOAA Optimum Interpolation (OI) SST (Reynolds et al., 2002) (http://www.emc.ncep.noaa.gov/research/cmb/sst_analysis/). The winter SST anomaly is calculated by setting the summer SST anomaly to zero and then smoothed by a digital filtering technique (Thoning et al., 1989) with a cut-off frequency of 0.6 cycles yr^{-1}. We see a general similarity in the variations of the winter APO change and the winter SST anomaly; for example, there are large corresponding peaks in 1999, followed by a sharp decrease in 2000 and a gradual increase thereafter with minor dips in 2003 and 2005. Note that the summer SST anomaly does not show such similarities to both the winter and summer APO changes. The relation between the winter SST anomaly and the winter APO change is easily understandable if lower SST anomaly in winter causes more vigorous ventilation. Indeed, these results seem to indicate that the APO changes at our sites are strongly affected by the regional fluxes influenced by winter SST anomaly near our sites. McKinley et al. (2003) examined interannual variability of the global air–sea O_2 flux during the period of 1980–1998 by using a biogeochemical ocean model. Their model simulation indicated that the global flux variability is primarily influenced by the El Nino/Southern Oscillation cycle in the equatorial Pacific and by the wintertime convection in the North Atlantic. However, our results seem to suggest that the wintertime convection in the western North Pacific also contribute to the global O_2 flux variability, or at least to the regional APO variability.

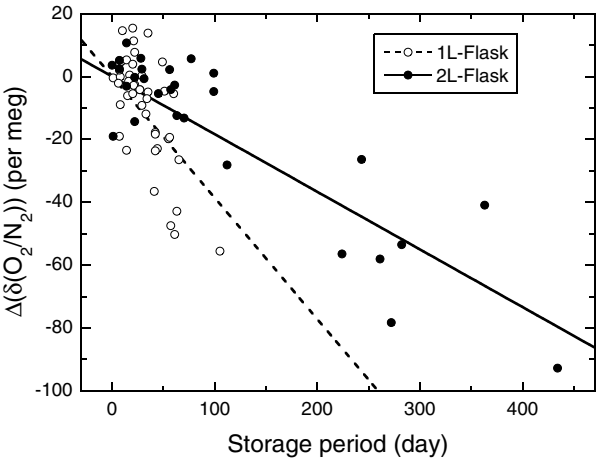

Fig. 6. Changes in $\delta(O_2/N_2)$ due to storage for the 1-l (open circle) and 2-l flasks (closed circle). The difference in the $\delta(O_2/N_2)$ between the first and the second measurements is plotted against the storage time. The lines are the linear regression fits constrained to pass through the origin.

4. Conclusion

We have estimated the oceanic and land biotic carbon sinks by using APO from two monitoring sites, HAT and COI, in Japan, and the global atmospheric CO_2 observation from the NOAA/ESRL GMD network. The oceanic and land biotic carbon sinks are found to be 2.4 ± 0.7 and 0.5 ± 0.9 Pg C yr^{-1}, respectively, for the 7-yr period between July 1998 and July 2005, and 2.1 ± 0.7 and 1.0 ± 0.9 Pg C yr^{-1}, respectively, for the 6-yr period between July 1999 and July 2005. The former estimates are based on data from HAT, and the latter estimates are based on combined data from HAT and COI. Our estimates agree, within the uncertainties, with recent estimates based on the decadal O_2/N_2 measurements by Bender et al. (2005) for July 1993–July 2002 and Manning and Keeling (2006) for January 1993–January 2003. In our estimation, we have adopted the ocean outgassing correction of 0.48 Pg C yr^{-1}, which is the same value Manning and Keeling (2006) adopted. The NIES O_2/N_2 scale is based on three reference cylinders for the period 1997–2001, and 11 reference cylinders for the period 2001–2005. We have evaluated the uncertainty in the NIES scale for the whole period to be ± 1 per meg yr^{-1}.

The rate of change in the deseasonalized trend of APO at HAT and COI show large interannual variability. Since these variations in APO are too large to be ascribed to the interannual variation in the oceanic CO_2 uptake, the cause of the APO change is likely due to changes in the oceanic O_2 fluxes. We find that the wintertime anomalies explain much of the interannual variability in APO trends, especially for COI. The variations in the winter SST anomaly in the northwestern North Pacific region (36–50°N, 144–180°E) show a similar pattern of variation to that of the rates of change in APO at both sites. These results seem to suggest that the O_2 flux associated with the ocean convection during winter mainly cause the interannual variability in APO at our sites. Although this feature is a disadvantage for calculation of the fossil CO_2 partitioning, our observation is useful in understanding more about the processes determining the atmospheric oxygen variations.

5. Acknowledgments

We are grateful to Fujio Shimano and Nobukazu Oda of the Global Environmental Forum and the local staffs for their continuous support in sample collection. Thanks are also expressed to Hisayo Sandanbata, Junko Tatematsu, Yoko Kajita and Fumiko Endo for their assistance in the CO_2 measurements and flask preparations. We thank Pieter Tans and Tom Conway for providing the globally averaged CO_2 data from the NOAA/ESRL GMD flask sampling network. Three anonymous reviewers made valuable comments that helped to improve the manuscript considerably. This work was financially supported by the Ministry of the Environment through the Global Environment Research Coordination System (FY 2001–2003 and FY 2004–2008).

6. Appendix: Evaluation of decreasing rate of $\delta(O_2/N_2)$ due to storage in glass flasks equipped with two single O-ring valves

Our 1- and 2-l glass flasks used for air sampling are equipped with two cylindrical shaft valves (Koshinrikagaku Seisakujo, Tokyo, Japan). A Viton® O-ring on the shaft seals the flask volume from the ambient air. The rate of decrease in $\delta(O_2/N_2)$ in each flask during the storage period was evaluated as follows. First, the glass flasks were filled with dry air from high pressure cylinders to a pressure of 0.25–0.3 MPa. Then the O_2/N_2 ratio in each flask was measured by GC/TCD until the pressure in the flask decreased to about 0.2 MPa, which is the usual sampling pressure. The O_2/N_2 ratios of the flasks were measured again after storage. The changes in the O_2/N_2 ratio between the first and second measurements are plotted against the individual storage periods in Fig. 6. The slopes of the linear regression lines constrained to pass through the origin (the (0,0) point) are -0.39 per meg d^{-1} for the 1-l flasks and -0.18 per meg d^{-1} for the 2-l flasks. The difference is due to the difference in the volume size of the flasks involved. Taking into account the flask volume, the sampling pressure, and the O-ring geometry (thickness: $\sim$2 mm, surface area: $\sim$20 mm^2) and material (Viton®), we find that the O_2/N_2 drift rates of our flasks are consistent with those reported by Sturm et al. (2004).

References

Balkanski, Y., Monfray, P., Battle, M. and Heimann, M. 1999. Ocean primary production derived from satellite data: an evaluation with atmospheric oxygen measurements. *Global Biogeochem. Cycles* **13**, 257–271.

Battle, M., Bender, M. L., Tans, P. P., White, J. W. C., Ellis, J. T. and co-authors. 2000. Global carbon sinks and their variability inferred from atmospheric O_2 and $d^{13}C$. *Science* **287**, 2467–2470.

Battle, M., Fletcher, S. M., Bender, M. L., Keeling, R. F., Manning, A. C. and co-authors. 2006. Atmospheric potential oxygen: new observations and their implications for some atmospheric and oceanic models. *Global Biogeochem. Cycles* **20**, GB1010, doi:10.1029/2005GB002534.

Bender, M., Ellis, T., Tans, P., Francey, R. and Lowe, D. 1996. Variability in the O_2/N_2 ratio of southern hemisphere air, 1991–1994: implications for the carbon cycle. *Global Biogeochem. Cycles* **10**, 9–21.

Bender, M. L., Ho, D. T., Hendricks, M. B., Mika, R., Battle, M. O.,, and co-authors. 2005. Atmospheric O_2/N_2 changes, 1993–2002: implications for the partitioning of fossil fuel CO_2 sequestration. *Global Biogeochem. Cycles* **19**, GB4017, doi:10.1029/2004GB002410.

Bopp, L., Le Quéré, C., Heimann, M., Manning, A. C. and Monfray, P. 2002. Climate-induced oceanic oxygen fluxes: implications for the contemporary carbon budget. *Global Biogeochem. Cycles* **16**(2), 1022, doi:10.1029/2001GB001445.

Conway, T. J., Tans, P. P., Waterman, L. S., Thoning, K. W., Kitzis, D. R. and co-authors. 1994. Evidence for interannual variability of the carbon cycle from the National Oceanic and Atmospheric Administration/Climate Monitoring and Diagnostics laboratory Global Air Sampling Network. *J. Geophys. Res.* **99**, 22,831–22,855.

Garcia, H. E., Boyer, T. P., Levitus, S., Locarnini, R. A. and Antonov, J. 2005. On the variability of dissolved oxygen and apparent oxygen utilization content for the upper world ocean: 1955 to 1998. *Geophys. Res. Lett.* **32**, L09604, doi:10.1029/2004GL022286.

Gruber, N., Gloor, M., Fan, S.-M. and Sarmiento, J. L. 2001. Air-sea flux of oxygen estimated from bulk data: implications for the marine and atmospheric oxygen. *Global Biogeochem. Cycles* **15**, 783–803.

Ishidoya, S., Sugawara, S., Hashida, G.., Morimoto, S., Aoki, S. and co-authors. 2006. Vertical profiles of the O_2/N_2 ratio in the stratosphere over Japan and Antarctica. *Geophys. Res. Lett.* **33**, L13701, doi:10.1029/2006GL025886.

Keeling, R. F. 1988. Development of an Interferometric Oxygen Analyzer for Precise Measurement of the Atmospheric O_2 Mole Fraction. Ph.D. Thesis. Harvard Univ., Cambridge, Mass., USA, pp. 178.

Keeling, R. F. and Shertz, S. R. 1992. Seasonal and interannual variations in atmospheric oxygen and implications for the global carbon cycle. *Nature* **358**, 723–727.

Keeling, R. F. and Garcia, H. E. 2002. The change in oceanic O_2 inventory associated with recent global warming. *Proc. Natl. Acad. Sci. U. S. A.* **99**, 7848–7853.

Keeling, R. F., Najjar, R. P., Bender, M. L. and Tans, P. P. 1993. What atmospheric oxygen measurements can tell us about the global carbon cycle. *Global Biogeochem. Cycles* **7**, 37–67.

Keeling, R. F., Piper, S. C. and Heimann, M. 1996. Global and hemispheric CO_2 sinks deduced from changes in atmospheric O_2 concentration. *Nature* **381**, 218–221.

Keeling, R. F., Manning, A. C., McEvoy, E. M. and Shertz, S. R. 1998a. Methods for measuring changes in atmospheric O_2 concentration and their application in southern hemisphere air. *J. Geophys. Res.* **103**, 3381–3397.

Keeling, R. F., Stephens, B. B., Najjar, R. G., Doney, S. C., Archer, D., and co-authors. 1998b. Seasonal variation in the atmospheric O_2/N_2 ratio in relation to the kinetics of air-sea gas exchange. *Global Biogeochem. Cycles* **12**, 141–163.

Keeling, R. F., Manning, A. C., Paplawsky, W. J. and Cox, A. C. 2007. On the long-term stability of reference gases for atmospheric O_2/N_2 measurements. *Tellus* **59B**, 3–14.

Langenfelds, R. L., Francey, R. J., Steele, L. P., Battle, M., Keeling, R. F., and co-authors. 1999. Partitioning of the global fossil CO_2 sink using a 19-year trend in atmospheric O_2. *Geophys. Res. Lett.* **26**, 1897–1900.

Le Quéré, C., Aumont, O., Bopp, L., Bousquet, P., Ciais, P. and co-authors. 2003. Two decades of ocean CO_2 sink and variability. *Tellus* **55B**, 649–656.

Levitus, S., Antonov, J. I., Boyer, T. P. and Stephens, C. 2000. Warming of the world ocean. *Science* **287**, 2225–2229.

Lombard, A., Garcia, D., Ramillien, G., Cazenave, A., Biancale, R. and co-authors. 2007. Estimation of steric sea level variations from combined GRACE and Jason-1 data. *Earth Planet. Sci. Lett.* **254**, 194–202.

Lyman, J. M., Willis, J. K. and Johnson, G. C. 2006. Recent cooling of the upper ocean. *Geophys. Res. Lett.* **33**, L18604, doi:10.1029/2006GL027033.

Mannning, A. C. and Keeling, R. F. 2006. Global oceanic and biotic carbon sinks from the Scripps atmospheric oxygen flask sampling network. *Tellus* **58B**, 95–116.

Marland, G. and Rotty, R. M. 1984. Carbon dioxide emissions from fossil fuels: a procedure for estimation and results for 1950–1982. *Tellus* **36B**, 232–261.

Marland, G.., Boden, T. A. and Andres, R. J. 2006. Global, Regional, and National CO_2 Emissions. In *Trends: A Compendium of Data on Global Change*. Carbon Dioxide Information Analysis Center, Oak Ridge National Laboratory, U.S. Department of Energy, Oak Ridge, Tenn., USA.

McKinley, G. A., Follows, M. J., Marchall, J. and Fan, S.-M. 2003. Interannual variability of air-sea O_2 fluxes and the determination of CO_2 sinks using atmospheric O_2/N_2. *Geophys. Res. Lett.* **30**(3), 1101, doi:10.1029/2002GL016044.

McKinley, G. A., Rödenbeck, C., Gloor, M., Houweling, S. and Heimann, M. 2004. Pacific dominance to global air-sea CO_2 flux variability: a novel atmospheric inversion agrees with ocean models. *Geophys. Res. Lett.* **31**, L22308, doi:10.1029/2004GL021069.

Patra, P. K., Maksyutov, S., Ishizawa, M., Nakazawa, T., Takahashi, T., and co-authors. 2005. Interannual and decadal changes in the sea-air CO_2 flux from atmospheric CO_2 inverse modeling. *Global Biogeochem. Cycles* **19**, GB4013, doi:10.1029/2004GB002257.

Plattner, G. K., Joos, F. and Stocker, T. F. 2002. Revision of the global carbon budget due to changing air-sea oxygen fluxes. *Global Biogeochem. Cycles* **16**(4), 1096, doi:10.1029/2001GB001746.

Reynolds, R. W., Rayner, N. A., Smith, T. M., Stokes, D. C. and Wang, W. 2002. An improved in situ and satellite SST analysis for climate. *J. Climate* **15**, 1609–1625.

Schiermeier, Q. 2007. Artefacts in ocean data hide rizing temperatures. *Nature* **447**, 8–9, doi:10.1038/447008a.

Severinghaus, J. P. 1995. *Studies of the Terrestrial O_2 and Carbon Cycles in Sand Dune Gases and in Biosphere 2*. Ph.D. Thesis, pp. 148, Columbia Univ., New York, NY.

Stephens, B. B., Keeling, R. F., Heimann, M., Six, K. D., Murnane, R., and co-authors. 1998. Testing global ocean carbon cycle models using measurements of atmospheric O_2 and CO_2 concentration. *Global Biogeochem. Cycles* **12**, 213–230.

Sturm, P., Leuenberger, M., Sirignano, C., Neubert, R. E. M., Meijer, H. A. J. and co-authors. 2004. Permeation of atmospheric gases through Viton O-rings used for flask sampling. *J. Geophys. Res.* **109**, D04309, doi:10.1029/2003JD004073.

Sturm, P., Leuenberger, M. and Schmidt, M. 2005. Atmospheric O_2, CO_2 and $\delta^{13}C$ observations from the remote sites Jungfraujoch, Switzerland, and Puy de Dôme, France. *Geophys. Res. Lett.* **32**, L17811, doi:10.1029/2005GL023304.

Thoning, K. W., Tans, P. P. and Komhyr, W. D. 1989. Atmospheric carbon dioxide at Mauna Loa Observatory 2. Analysis of the NOAA GMCC data, 1974–1985. *J.Geophys. Res.* **94**, 8549–8565.

Tohjima, Y. 2000. Method for measuring changes in the atmospheric O_2/N_2 ratio by a gas chromatograph equipped with a thermal conductivity detector. *J. Geophys. Res.* **105**, 14575–14584.

Tohjima, Y., Machida, T., Utiyama, M., Katsumoto, M., Fujinuma, Y. and Maksyutov, S. 2002. Analysis and presentation of in situ atmospheric methane measurements from Cape Ochi-ishi and Hateruma Island. *J. Geophys. Res.* **107**(D12), 4148, doi:10.1029/2001JD001003.

Tohjima, Y., Mukai, H., Machida, T. and Nojiri, Y. 2003. Gas-chromatographic measurements of the atmospheric oxygen/nitrogen ratio at Hateruma Island and Cape Ochi-ishi, Japan. *Geophys. Res. Lett.* **30**(12), 1653, doi:10.1029/2003GL017282.

Tohjima, Y., Machida, T., Watai, T., Akama, I., Amari, T., and co-authors. 2005a. Preparation of gravimetric standards for measurements of atmospheric oxygen and re-evaluation of atmospheric oxygen concentration. *J. Geophys. Res.* **110**, D11302, doi:10.1029/2004JD005595.

Tohjima, Y., Mukai, H., Machida, T., Nojiri, Y. and Gloor, M. 2005b. First measurements of the latitudinal atmospheric O_2 and CO_2 distributions across the western Pacific. *Geophys. Res. Lett.* **32**, L17805, doi:10.1029/2005GL023311.

Trenberth, K. E. and Smith, L. 2005. The mass of the atmosphere: a constraint on global analyses. *J. Climate* **18**, 864–875.

Willis, J. K., Roemmich, D. and Cornuelle, B. 2004. Interannual variability in upper ocean heat content, temperature, and thermosteric expansion on global scales. *J. Geophys. Res.* **109**, C12036, doi:10.1029/2003JC002260.